Table 1. Polymerase chain reaction primers used in this study

Genes	Sense	Antisense
TNNT2	5′-GAAACAGGATCAACGACAACCA-3′	5′-CGCCCGGTGACTTTGG-3′
TNNC1	5′-GATCTCTTCCGCATGTTTGACA-3′	5′-TGGCCTGCAGCATCATCTT-3′
TNNC2	5′-AGATCGAATCCCTGATGAAGGA-3′	5′-CATCTTCAGAAACTCGTCGAAGTC-3′
GAPDH	5′-CTACCCCCAATGTATCCGTTGT-3′	5′-TAGCCCAGGATGCCCTTTAGT-3′

GAPDH, Glyceraldehyde 3 phosphate dehydrogenase

Table 2. Summary of voltage potentials for cardiomyocytes cultured in several types of extracellular matrix-coated dishes

Substrate	Action potential (mV) [Beating rate (Hz)]		
	Day 7	Day 14	Day 21
Gelatin	6.7 ± 0.49 [1.2 ± 0.05]	6.6 ± 1.26 [1.3 ± 0.01]	3.1 ± 0.21[2.8 ± 0.03]
Fibronectin	1.1 ± 0.97 [1.1 ± 0.30]	6.9 ± 1.15 [1.3 ± 0.42]	2.8 ± 0.11[2.0 ± 0.11]
Collagen type-I	2.6 ± 0.35 [0.8 ± 0.02]	1.7 ± 0.03 [2.3 ± 0.05]	ND
Polystyrene	2.0 ± 0.75 [0.3 ± 0.04]	ND	ND

ND, not done

tion mixture was heated at 94°C for 5 min to inactivate the enzyme and cooled at 4°C for 15 min. The RNase (DNase-free, 0.5 μg, Roche Diagnostics, Mannheim, Germany) was added to the mixture and incubated at 37°C to remove the template of RNA.

Real-time quantitative polymerase chain reaction

Real-time quantitative polymerase chain reaction (PCR) was conducted with SYBR Green. Primers for PCR analysis for troponin T type-2, troponin C type-1, and troponin C type-2 were designed using Primer Express software (Perkin-Elmer Applied Biosystems, Warrington, UK). The primer sequences are shown in Table 1. The reaction mixtures contained 23.74 μl distilled water, 25 μl SYBR Green Realtime PCR master mix (Toyobo), 100 nM of each primer, and 0.26 μl cDNA. The thermal profile for PCR was 50°C for 2 min, followed by 95°C for 10 min, followed by 40 cycles of 15 s at 95°C and 1 min at 60°C. Distilled water 0.26 μl was used as a negative control PCR reaction to ensure the absence of template contamination in PCR reagents. The average threshold cycle (Ct) values of triplicate measurements were used for all subsequent calculations on the basis of the delta Ct method.

Results

Beating behavior of isolated cardiomyocytes

One week after culture, the action potential of cardiomyocytes on gelatin-coated dishes was higher than that for other conditions (Fig. 1), and the beating duration was also longer than that for other conditions. The action potential and beating rates on each matrix are summarized in Table 2. After 7 days of culture, the action potential was around 6.7 ± 0.49 mV for cardiomyocytes cultured on gelatin-coated dishes, 1.1 ± 0.97 mV on fibronectin-coated dishes, 2.0 ± 0.35 mV on collagen type I-coated dishes, and 2.0 ± 0.75 mV on noncoated polystyrene dishes. These results indicate that the beating rate on fibronectin-coated dishes, collagen type I-coated dishes, and noncoated polystyrene dishes were 84%, 61%, and 70% lower than the beating rate on gelatin-coated dishes after 1 week of cultivation.

After 14 days of culture, the action potential became 6.6 ± 1.26 mV on gelatin-coated dishes, 6.9 ± 1.15 mV on fibronectin-coated dishes, and 1.7 ± 0.03 mV on collagen type I-coated dishes. No beating was observed on noncoated polystyrene dishes after 2 weeks of cultivation. After 21 days of culture, the action potential was 3.1 ± 0.21 mV on gelatin-coated and 2.8 ± 0.11 mV on fibronectin-coated dishes. No action potential was detected on collagen type I-coated dishes and polystyrene dishes.

The beating rate of cardiomyocytes was also affected by the ECM proteins. After 7 days of culture, the beating rate of cardiomyocytes was 1.2 ± 0.05 Hz on gelatin-coated dishes, 1.1 ± 0.3 Hz on fibronectin-coated dishes, 0.8 ± 0.02 Hz on collagen type I-coated dishes, and 0.3 ± 0.04 Hz on noncoated polystyrene dishes. After 14 days of culture, the beating rate became 1.3 ± 0.01 Hz on gelatin-coated dishes, 1.3 ± 0.42 Hz on fibronectin-coated dishes, and 2.3 ± 0.05 Hz on collagen type I-coated dishes. After 21 days, the beating rate was 2.8 ± 0.03 Hz on gelatin-coated dishes and 2.0 ± 0.11 Hz on fibronectin-coated dishes, whereas cardiomyocytes cultured on noncoated polystyrene dishes and collagen-coated dishes did not beat well and stopped at an early stage of cultivation. These results indicate that gelatin could maintain the beating behavior of cardiomyocytes for a longer time compared to fibronectin or collagen type I.

Expression of troponin T type-2 and troponin C type-1

Cardiac troponin T type-2 and troponin C type-1 are known to be cardiomyocyte markers and are important in the structure of muscle tissue; they also play a role in the contraction of muscle cells.[13] After 4 weeks of culture,

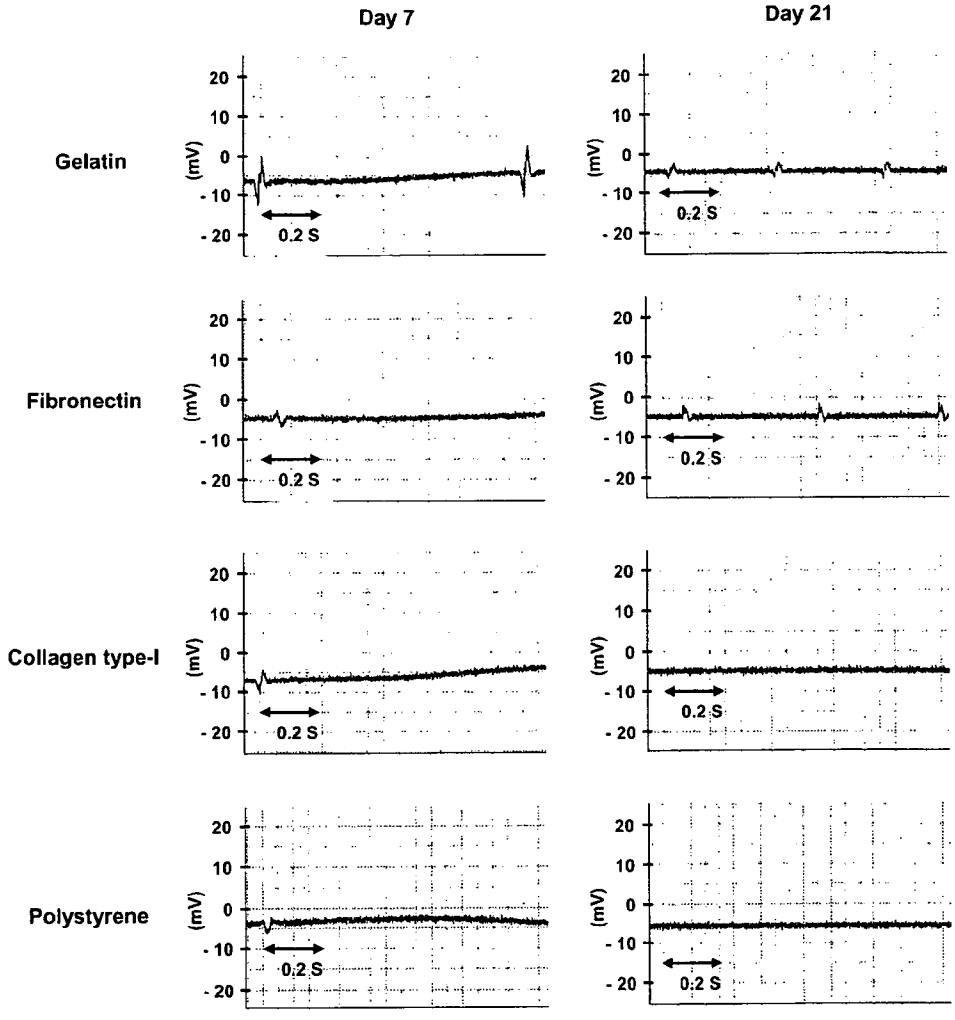

Fig. 1. Electrophysiological assessment of isolated cardiomyocytes after 7 and 21 days of cultivation on different substrates

expression of troponin T type-2 in cardiomyocytes on gelatin-coated dishes was 7, 6, and 12 times higher than those on fibronectin-coated, collagen-coated, and non-coated dishes (Fig. 2A). Expression of troponin C type-1 on gelatin-coated dishes was also 5, 6, and 32 times higher than those on fibronectin-coated, collagen type I-coated, and noncoated dishes (Fig. 2B). These results are consistent with the results of the electrophysiological study (Fig. 1), in which the beating of cardiomyocytes still could be detected on gelatin- and fibronectin-coated dishes after 3 weeks of cultivation.

Differentiation of P19.CL6 cells

Beating colonies were found on gelatin-coated dishes in 9 days with α-MEM medium containing 1% DMSO. This was followed by cells cultured on fibronectin-coated dishes after 10 days of culture and collagen type I-coated dishes after 11 days of culture. The average number of beating colonies found on the first day of detection was 13 ± 7 colonies per dish on gelatin-coated dishes, 9 ± 5 colonies per dish on fibronectin-coated dishes, 5 ± 2 colonies on collagen type I-coated dishes, and 3 ± 1 colonies on polystyrene dishes (Table 3).

As described earlier, troponin T type-2 and troponin C type-1 are known to be markers of cardiomyocytes,[13] and troponin C type-2 is reported to be a marker of cardiac development.[14] Expression of troponin T type 2 on gelatin- and fibronectin-coated dishes was higher than that for the other dishes, as shown in Fig. 3A. However, the expression of troponin C type-2 in collagen type I-coated dishes and noncoated polystyrene dishes was higher than that in gelatin- and fibronectin-coated dishes. The high expression of troponin C type-2 on collagen type I coated dishes and noncoated polystyrene dishes on day 11 was possibly because of the delayed differentiation of P19.CL6 cells to cardiomyocytes-like cells. Stoutamyer and Dhoot reported that troponin C type-2 was first expressed on day 3, reached maximum expression on day 5, and decreased day by day until no expression was found on day 11 during the development of quail heart in ovo.[14] Stoutamyer and Dhoot also reported that the expression of troponin C type-1 was detected on day 2 and decreased during the increase of

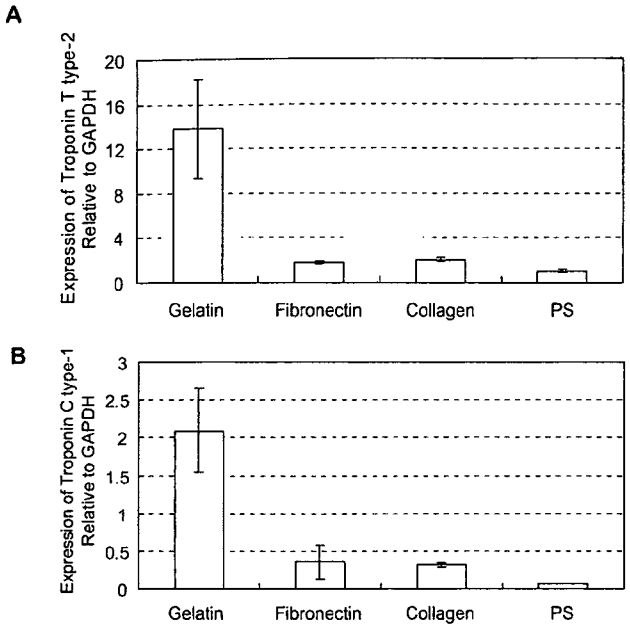

Fig. 2. Expression of cardiac markers (**A** troponin T type-2 and **B** troponin C type-1) in isolated cardiomyocytes after cultivation for 4 weeks on various types of extracellular matrix. *GAPDH*, Glyceraldehyde 3 phosphate dehydrogenase; *PS*, polystyrene

Table 3. Number of beating colonies of P19.CL6 cells 11 days after induction with 1% dimethyl sulfoxide

Substrate	Average number of beating colonies per dish
Gelatin	13 ± 7
Fibronectin	9 ± 5
Collagen type-I	5 ± 2
Polystyrene	3 ± 1

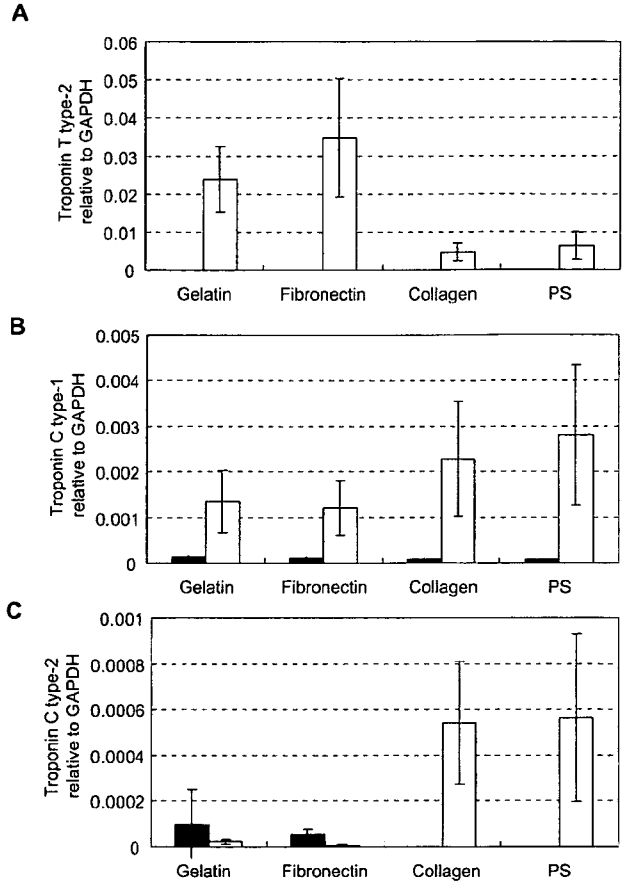

Fig. 3. Expression of cardiac markers in P19.CL6 cells (**A** troponin T type-2, **B** troponin C type-1, **C** troponin C type-2) treated with minimum essential medium alpha medium (α-MEM) containing 1% dimethyl sulfoxide on various dishes (*white bars*) or with α-MEM as a control for 11 days (*black bars*) PS, polysyrene

troponin C type-2, reaching a constant level after that.[14] In addition, the troponin C type-2 expression on a collagen-coated or noncoated dish may suggest skeletal muscle differentiation of P19.CL6 cells, although further analysis is needed.

These results demonstrated that differentiation of P19.CL6 cells to beating cells on gelatin-coated dishes and fibronectin-coated dishes was faster and more effective than that on collagen type I-coated dishes and noncoated polystyrene dishes.

Discussion

In the present study, enhanced action potentials and elongated beating durations of neonatal cardiomyocyte were observed on gelatin-coated dishes compared to those on collagen type I-coated dishes. Possible differences between gelatin and collagen are: (1) collagen posses a triple-helical conformation, (2) gelatin has a wide molecular weight distribution depending on its preparation process, (3) gelatin is easily hydrolyzed by protease,[17] (4) the dynamic storage modulus of gelatin is higher than that of collagen,[18] and (5) gelatin binds with fibronectin with a higher affinity.[19–21] It has already been reported that fibronectin is a very elastic substrate.[22]

The mechanism of the elongated beating duration on gelatin-coated substrate is unclear, but the mechanical properties (elasticity) and biological activity of the substrates might be influential. It has been reported that the mechanical properties of culture matrices affect various cellular properties such as the morphology of embryonic stem cells,[23,24] the collagen production of fibroblasts,[25,26] and the differentiation of mesenchymal and neural stem cells.[27,28]

Fibronectin produced by culture cells is known to associate with the fibronectin-binding domain of collagen, resulting in fibrillogenesis.[21] It has also been reported that fibronectin binds to gelatin more strongly than to collagen.[20,21] Therefore, the high production of fibrils might occur more effectively on gelatin-coated dishes than on fibronectin- or collagen-coated dishes. These connecting elastic fibers might regulate the motion of cardiomyocytes during

contraction and recoil, as suggested by Ahumada and Saffitz.[29] The highly elastic features of matrices made of gelatin, fibronectin bound onto gelatin,[18,22] and developed fibrin matrices may allow easier contraction of cardiomyocytes, leading to larger action potentials and longer beating durations on gelatin.

P19.CL6 cells were used to study the effect of culture substrates on cardiogenesis in vitro because Ohkubo reported that P19.CL6 cells differentiated into cardiomyocytes in 10 days after DMSO treatment, and observation of differentiation continued for 11 days. The first beating colony was found on the 9th day on gelatin-coated dishes, on the 10th day on fibronectin-coated dishes, and on the 11th day on collagen type I-coated dishes and noncoated polystyrene dishes. The expressions of troponin T type-2 on gelatin- and fibronectin-coated dishes were significantly higher than those on collagen type I-coated dishes and on noncoated polystyrene dishes. High expression of troponin C type-2 in collagen type I-coated dishes and noncoated polystyrene dishes is considered to indicate delayed cardiac differentiation or skeletal muscle differentiation of P19. CL6.

The differentiation of P19.CL6 cells on gelatin- and collagen type I-coated dishes was very different, despite their similar unit structure. The fast differentiation on gelatin was possibly because of slow cell proliferation on high-dynamic-storage-modulus substrates.[18] The growth of P19.CL6 cells on gelatin-coated dishes was about half that on collagen type I-coated dishes (data not shown). Walsh et al. suggested that the proliferation of mesenchymal stem cells was suppressed during the differentiation to osteoblasts in vitro.[30] The fast differentiation on fibronectin-coated dishes may also relate to the elasticity of the substrate.[22]

This finding will hopefully offer a bright future for the myocardial patch scaffold. It has been reported that the probability of cardiac differentiation of adipose tissue-derived mesenchymal stem cells after transplantation to infracted rat heart is quite low.[31] In the present study, the gelatin-based niche was found to be preferable for cardiac differentiation and for the beating function of cardiomyocytes. We will be applying these results to the cardiac differentiation of mesenchymal stem cells in order to prepare allogeneic beating cardiomyocytes.

Conclusion

The physical and biological properties of the substrate were the important factors not only for maintaining cardiac functions but also for leading to the cardiac differentiation of P19.CL cells. Gelatin was found to be a promising ECM protein to this end in vitro.

Acknowledgments This work was partly supported by a Grant-in-Aid for Scientific Research (B) from the Ministry of Education, Culture, Sports, Science and Technology of Japan. The author (Azizi Miskon) would like to thank the Ministry of Higher Education, Malaysia, and Tun Hussein Onn of the University of Malaysia for funding his study under the Academic Training Scheme.

References

1. Li RK, Mickle DA, Weisel RD, Zhang J, Mohabeer MK. In vivo survival and function of transplanted rat cardiomyocytes. Circ Res 1996;78:283–288
2. El Oakley RM, Ooi OC, Bongso A, Yacoub MH. Myocyte transplantation for myocardial repair: a few good cells can mend a broken heart. Ann Thorac Surg 2001;71:1724–1733
3. Ott HC, Davis BH, Taylor DA. Cell therapy for heart failure – muscle, bone marrow, blood, and cardiac-derived stem cells. Semin Thorac Cardiovasc Surg 2005;17:348–360
4. Segers VF, Lee RT. Stem-cell therapy for cardiac disease. Nature 2008;451:937–942
5. Makino S, Fukuda K, Miyoshi S, Konishi F, Kodama H, Pan J, Sano M, Takahashi T, Hori S, Abe H, Hata J, Umezawa A, Ogawa S. Cardiomyocytes can be generated from marrow stromal cells in vitro. J Clin Invest 1999;103:697–705
6. Wakitani S, Saito T, Caplan AI. Myogenic cells derived from rat bone marrow mesenchymal stem cells exposed to 5-azacytidine. Muscle Nerve 1995;18:1417–1426
7. Xu W, ZhangX, Qian H, Zhu W, Sun X, Hu J, Zhou H, Chen Y. Mesenchymal stem cells from adult human bone marrow differentiate into a cardiomyocyte phenotype in vitro. Exp Biol Med 2004; 229:623–631
8. Zhang FB, Li L, Fang B, Zhu DL, Yang HT, Gao PJ. Passage-restricted differentiation potential of mesenchymal stem cells into cardiomyocyte-like cells. BBRC 2005;336:784–792
9. Liu Y, Song J, Liu W, Wan Y, Chen X, Hu C. Growth and differentiation of rat bone marrow stromal cells: does 5-azacytidine trigger their cardiomyogenic differentiation? Cardiovasc Res 2003;58:460–468
10. Macfelda K, Kapeller B, Wilbacher I, Losert UM. Behavior of cardiomyocytes and skeletal muscle cells on different extracellular matrix components – relevance for cardiac tissue engineering. Artif Organs 2007;31:4–12
11. Bird SD, Doevendans PA, van Rooijen MA, Brutel de la Riviere A, Hassink RJ, Passier R, Mummery CL. The human adult cardiomyocyte phenotype. Cardiovasc Res 2003;58:423–434
12. Ohkubo AH. Differentiation of beating cardiac muscle cells from a derivative of P19 embryonal carcinoma cells. Cell Struct Funct 1996;21:101–110
13. Saggin L, Ausoni S, Gorza L, Sartore S, Schiaffino S. Troponin T switching in the developing rat heart. J Biol Chem 1998;263: 18488–18492
14. Stoutamyer A, Dhoot GK. Transient expression of fast troponin C transcripts in embryonic quail heart. J Muscle Res Cell Motil 2005;26:237–245
15. Seglen PO. Preparation of isolated rat liver cells. Methods Cell Biol 1976;13:29–83
16. Moldeus P, Högberg J, Orrenius S. Isolation and use of liver cells. Methods Enzymol 1978;52:60–71
17. Zhang Z, Li G, Shi B. Physicochemical properties of collagen, gelatin, and collagen hydrolysate derived from bovine limed split wastes. J Soc Leather Technol Chem 2006;90:23–28
18. Chien JC, Chang EP. Dynamic mechanical and rheo-optical studies of collagen and gelatin. Biopolymers 1972;11:2015–2031
19. Little CD, Chen WT. Masking of extracellular collagen and the co-distribution of collagen and fibronectin during matrix formation by cultured embryonic fibroblast. J Cell Sci 1982;55: 35–50
20. Engvall E, Ruoslahti E, Miller ED. Affinity of fibronectin to collagens of different genetic types and to fibrinogen. J Exp Med 1978;147:1584–1595
21. Dzamba BJ, Wu H, Jaenisch R, Peters DM. Fibronectin binding site in type I collagen regulates fibronectin fibril formation. J Cell Biol 1993;121:1165–1172
22. Erickson HP. Stretching fibronectin. J Muscle Res Cell Motil 2002;23:575–580
23. Bard JB, Hay ED. The behavior of fibroblasts from the developing avian cornea. Morphology and movement in situ and in vitro. J Cell Biol 1975;67:400–418
24. Hay ED. Interaction of embryonic surface and cytoskeleton with extracellular matrix. Am J Anat 1982;165:1–12

25. Nakagawa S, Pawelek P, Grinnell F. Extracellular matrix organization modulates fibroblast growth and growth factor responsiveness. Exp Cell Res 1989;182:572–582
26. Halliday NL, Tomasek JJ. Mechanical properties of the extracellular matrix influence fibronectin fibril assembly in vitro. Exp Cell Res 1995;217:109–117
27. Engler AJ, Sen S, Sweeney HL, Discher DE. Matrix elasticity directs stem cell lineage specification. Cell 2006;126:677–689
28. Saha K, Keung AJ, Irwin EF, Li Y, Little L, Schaffer DV, Healy KE. Substrate modulus directs neural stem cell behavior. Biophys J 2008;95:4426–4438
29. Ahumada GG, Saffitz JE. Fibronectin in rat heart: a link between cardiac myocytes and collagen. J Histochem Cyotchem 1984;4: 383–388
30. Walsh S, Jordan GR, Jefferiss C, Stewart K, Beresford JN. High concentrations of dexamethasone suppress the proliferation but not the differentiation or further maturation of human osteoblast precursors in vitro: relevance to glucocorticoid-induced osteoporosis. Rheumatology 2001;40:74–83
31. Miyahara Y, Nagaya N, Kataoka M, Yanagawa B, Tanaka K, Hao H, Ishino K, Ishida H, Shimizu T, Kangawa K, Sano S, Okano T, Kitamura S, Mori H. Monolayered mesenchymal stem cells repair scarred myocardium after myocardial infarction. Nat Med 2006;12: 459–465

Biomacromolecules

Article

In Vivo Tissue Response and Degradation Behavior of PLLA and Stereocomplexed PLA Nanofibers

Daisuke Ishii, Tang Hui Ying, Atsushi Mahara, Sunao Murakami, Tetsuji Yamaoka, Won-ki Lee, and Tadahisa Iwata

Biomacromolecules, **2009**, 10 (2), 237-242• DOI: 10.1021/bm8009363 • Publication Date (Web): 31 December 2008

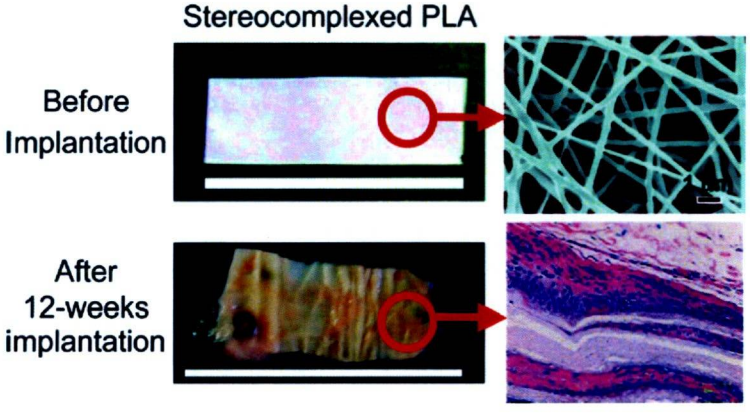

More About This Article

Additional resources and features associated with this article are available within the HTML version:

- Supporting Information
- Access to high resolution figures
- Links to articles and content related to this article
- Copyright permission to reproduce figures and/or text from this article

View the Full Text HTML

Biomacromolecules is published by the American Chemical Society. 1155 Sixteenth Street N.W., Washington, DC 20036

In Vivo Tissue Response and Degradation Behavior of PLLA and Stereocomplexed PLA Nanofibers

Daisuke Ishii,[†,‡] Tang Hui Ying,[†,§,||] Atsushi Mahara,[⊥] Sunao Murakami,[⊥] Tetsuji Yamaoka,[⊥] Won-ki Lee,[▽] and Tadahisa Iwata*[,†,○]

Polymer Chemistry Laboratory, RIKEN Institute, 2-1 Hirosawa, Wako-shi, Saitama 351-0198, Japan, School of Biological Science, Universiti Sains Malaysia, 11800 Penang, Malaysia, Department of Biomedical Engineering, Advanced Medical Engineering Center, National Cardiovascular Center Research Institute, 5-7-1 Fujishirodai, Suita, Osaka 565-8565, Japan, and Division of Chemical Engineering, Pukyong National University, San 100, Yongdang-dong, Nam-gu, Busan 608-739, Republic of Korea

Received August 21, 2008; Revised Manuscript Received November 24, 2008

Biocompatibility of PLLA and stereocomplexed PLA nanofibers was evaluated by subcutaneous implantation in rats for 4−12 weeks. Characterization of the nanofibers was performed by GPC, SEM, wide-angle X-ray diffraction, and optical microscopy of hematoxylin-eosin stained ultrathin sections of explanted nanofibers. Stereocomplexed PLA nanofiber showed slower degradation than PLLA nanofiber and thus retained their shape after prolonged implantation. Furthermore, stereocomplexed PLA nanofiber caused milder inflammatory reaction than PLLA nanofiber. These results offer the potential use of PLLA and stereocomplexed PLA nanofibers as a biomaterial for short-term and long-term tissue regeneration, respectively. Stereocomplexed PLA nanofiber after in vitro degradation showed smaller degree of swelling than PLLA nanofiber. Taking the results of in vivo degradation together with in vitro degradation into consideration, bioabsorption mechanism of the in vivo degradation of the nanofibers is proposed.

Introduction

In the field of medical sciences, the method of tissue engineering has been extensively studied to overcome the problems of conventional methods such as organ transplantation and usage of artificial organs.[1] In tissue engineering, the proliferation and differentiation of cultured cells for deficiency repair has to be artificially controlled. The development of scaffold materials on which cells proliferate and differentiate has been a major concern in tissue engineering. Conventionally, collagens and gelatins extracted from animals have been used to produce scaffolds. However, the usage of these animal-origin materials is shrinking for fear of infectious diseases. Alternatively, the usage of biodegradable and biocompatible polymers that do not contain infectious substances such as endotoxins and prions has been explored.

Recently, as a novel method for producing scaffolds, formation of nanofibers with the diameter ranging from several tens to hundreds of nanometers is extensively studied.[2−4] Nanofiber scaffolds have fine pores and grooves as small as a few micrometers wide. Such fine structural features facilitate the adhesion and proliferation of cells. It is required for nanofiber scaffolds to sustain sufficient strength to support regenerating tissue cells and to be degraded after the tissue regeneration is completed. To meet these demands, various kinds of biodegradable and biocompatible polymers have been processed into nanofibers. Furthermore, the fiber morphology, crystalline structure, and degradation behavior of the nanofibers have been investigated.[5−7]

Poly(lactide) (PLA) is one of a few polymers that is practically applied as various medical materials such as implants and sutures.[8] PLA possesses mechanical properties sufficient to endure the mechanical load applied in human body. However, it is readily hydrolyzed both in enzymatic and nonenzymatic conditions.[9] The high susceptibility of PLA toward hydrolysis becomes a shortcoming when the long-time storage under physiological conditions is required. Various efforts to overcome this shortcoming have been attempted. One of such efforts is the formation of stereocomplex in PLA materials.

Stereocomplexed PLA is a characteristic crystalline form of PLA.[10,11] A sterically stable racemic crystal of stereocomplexed PLA is formed by complexing poly(L-lactide) (PLLA) and poly(D-lactide) (PDLA) that take molecular conformations of left-handed and right-handed helices, respectively.[12] As a result, stereocomplexed PLA has a melting temperature of 230 °C, that is 50 °C higher than PLLA and PDLA.[10] Furthermore, it has been reported that stereocomplexed PLA is more stable against hydrolysis than PLLA.[13−15] This finding offers the possibility for controlling the hydrolytic behavior of PLA material by the formation of stereocomplex. Although various methods have been proposed and investigated for the formation of stereocomplex within PLA materials,[16,17] PLA materials that contain only racemic crystal has not yet been processed. Furthermore, the conventional processes involve long-time annealing at elevated temperatures as high as 180 °C and repeated stretching. To form stereocomplexed PLA more conveniently, electrospinning has recently been applied to the formation of stereocomplexed

* To whom correspondence should be addressed. Tel.: +81-3-5841-7888. Fax: +81-3-5841-1304. E-mail: atiwata@mail.ecc.u-tokyo.ac.jp.
† RIKEN Institute.
‡ Present affiliation and address: Department of Materials Chemistry, Faculty of Science and Technology, Ryukoku University 1-5 Yokotani, Seta Oe-cho, Otsu-shi, Shiga 520-2194, Japan.
§ Universiti Sains Malaysia.
|| Present affiliation and address: Bioengineering Laboratory, RIKEN Institute, 2-1 Hirosawa, Wako-shi, Saitama 351-0198, Japan.
⊥ National Cardiovascular Center Research Institute.
▽ Pukyong National University.
○ Present affiliation and address: Graduate School of Agricultural and Life Sciences, The University of Tokyo, 1-1-1 Yayoi, Bunkyo-ku, Tokyo 113-8657, Japan.

10.1021/bm8009363 CCC: $40.75
Published on Web 12/31/2008

PLA.[18] In particular, we have first succeeded in processing sterecomplexed PLA nanofiber in which the racemic crystal is only the crystalline polymorph.[19] The formation of racemic crystal was performed by annealing the as-spun nanofiber at 100 °C, which is 80 °C lower than those in previously reported studies.

The degradation behavior of PLA nanofibers has been investigated by using various specimens and conditions.[20−22] However, the previous reports were all limited to in vitro conditions. There have been no reports on the biocompatibility and in vivo degradation behavior of stereocomplexed PLA nanofibers.

In this work, tissue responses and degradation behavior of PLLA and stereocomplexed PLA nanofibers in vivo were investigated by subcutaneously implanting these nanofibers in rats. The tissue response against the nanofibers has been investigated by means of histological observation. The changes in structure and properties of the nanofibers during subcutaneous implantation has been investigated using scanning electron microscopy (SEM), wide-angle X-ray diffraction (WAXD), gel permeation chromatography (GPC), and mechanical tensile testing. The relation between tissue response and degradation behavior of nanofibers is discussed in terms of the structural and property changes of the nanofibers.

Experimental Section

Materials. PLLA with a M_n of 4.7 × 10^5 and M_w/M_n of 1.8 was purchased from Polysciences, Inc. and used as received. PDLA with a M_n = 2.2 × 10^5 and M_w/M_n of 1.5 was synthesized according to the following procedure. The D-lactide monomer, obtained from Purac, was recrystallized from anhydrous ethyl acetate. Bulk polymerizations were carried out in glass ampoules containing a magnetic stirring bar at 130 °C. Stannous octanoate in petroleum ether was used as the catalyst for the ring-opening polymerization. The ampoules were evacuated using a high vacuum pump and repeatedly flushed with high purity nitrogen to remove volatile impurities, solvents, and oxygen. Then the ampoules were sealed with a blowtorch and heated to the reaction temperature. The products in the ampoules were dissolved in chloroform, precipitated in the excess of methanol, filtered, and dried.

Electrospinning. Solutions of PLLA and PDLA (1 wt %) were prepared using 1,1,1,3,3,3-hexafluoro-2-propanol, HFIP, as the solvent. For the preparation of PLA stereocomplex nanofibers, equal volume of PLLA and PDLA solutions were mixed for several seconds by vortex mixer. Nanofibers were prepared using an Esprayer ES-2000 electrospinning device by Fuence, Co. Ltd. Dope solutions were extruded with a speed of 2.4 mL/h from a syringe needle with an inner diameter of 0.5 mm. Electrical voltage of 15 kV was applied to the syringe. Nanofibers were deposited onto a 10 × 10 cm^2 aluminum substrate placed perpendicular to the needle. To ensure sufficient thickness of nanofiber mats, the substrate was covered with a template made by a 51.4 μm thick Kapton film on which a 3 × 3 cm^2 window was opened. Distance between the needle tip and the substrate was set to 15 cm. The atmosphere of the spinning chamber was kept at less than 30% of relative humidity. PLLA and PLA stereocomplex nanofibers were then annealed in an oven at 100 °C for 8 h. Each electrospun PLA nanofiber mats was then cut into two different dimensions measuring 1 × 1 cm^2 and 1 × 3 cm^2, respectively. To prevent contamination, all scaffolds were sterilized overnight with ethylene oxide at 40 °C and kept in sealed bags until use.

Subcutaneous Implantation in Rat and Retrieval. Two 12-week old male Wistar rats were used for implanting the scaffolds; one for scaffolds measuring 1 × 1 cm^2, while the other for scaffolds measuring 1 × 3 cm^2. The experimental protocol had been approved by the Animal Care Committee of the National Cardiovascular Center, Osaka, Japan. The implantation of nanofiber mat was performed under anesthesia using diethyl ether. The 1 × 1 cm^2 scaffolds were implanted subcutaneously at one side of the backbone while the 1 × 3 cm^2 scaffolds were implanted subcutaneously at the backbone. The grouping of the rats was based on the duration of observation for 4 weeks and 12 weeks.

Upon explantation, the nanofiber mats measuring 1 × 1 cm^2 were excised with the surrounding tissues and stored in 2.5% glutaraldehyde in phosphate buffer saline (PBS) with a pH of 7 until further preparation of ultrathin section for histological observation. The retrieved 1 × 3 cm^2 nanofiber mats were treated with 1.25 wt % trypsin solution to remove the surrounding tissues. They were then kept in tubes containing PBS at 4 °C until further use. Trace amount of sodium azide was added to avoid the decay of the specimens. After trypsin treatment, surrounding tissues were manually removed as much as possible. The nanofiber mats were repeatedly washed using milli-Q water and dehydrated using ethanol series. Finally, the dehydrated nanofiber mats were dried overnight using vacuum desiccator at room temperature.

In Vitro Degradation. Nanofiber mats with the size of 1 × 3 cm^2 were incubated in 5 mL of PBS with a pH of 7.27 for 4−12 weeks at 37 °C. The medium was changed every 2 weeks. After 4 and 12 weeks of incubation, the nanofiber mats were washed thoroughly with distilled water, vacuum-dried at room temperature, and then subjected to SEM observation.

Histological Observation. The surrounding tissues were excised together with the implanted nanofiber mats and fixed with 2.5% glutaraldehyde in PBS with a pH of 7. A small piece of the tissue was then embedded in paraffin before subjecting it to microtome sectioning. Hematoxylin and eosin (HE) were used for staining the tissues. The tissue response to nanofiber mats was evaluated from the coloration observed with a phase-contrast microscope.

Scanning Electron Microscopy (SEM). Nanofiber mat was placed on a stub and then coated with Au. The thickness of Au coat was about 15 nm. SEM images of nanofibers were obtained using a field emission scanning electron microspope (JSM-6330F, JEOL, Co. Ltd.) operating at an acceleration voltage of 5 kV of and an emission current of 12 μA. For estimating the average diameter of nanofibers, diameter was measured at more than 60 points on the printed SEM image.

Wide-Angle X-ray Diffraction (WAXD). WAXD patterns of nanofiber mats were acquired under ambient condition using Rigaku RINT-2500 system operating at 40 kV and 200 mA. Measurements were performed on a Bragg−Brentano type $2\theta/\theta$ goniometer in a reflection mode. Ni-filtered Cu Kα radiation (λ = 0.15418 nm) was collimated with a 1/2 deg divergence slit, 1/6 deg scatter slit and 0.15 mm receiving slit. Scans were performed three times in a 2θ range of 10−40° with a scan rate of 0.5°/min and 0.05° step.

Gel Permeation Chromatography (GPC) Analysis. The molecular weight analysis of the nanofiber mats was performed with gel-permeation chromatography at 40 °C, using a Shimadzu LC-10A GPC system equipped with a RID-10A refractive index detector and Shodex K-806 M and K-802 columns. Chloroform was used as the eluent at a flow rate of 0.8 mL min^{-1}. The calibration curve was prepared by using monodisperse polystyrene standards.

Results

Changes in the Appearance of Nanofiber Mats During Subcutaneous Implantation. Figure 1a,b shows SEM images of the PLLA and stereocomplexed PLA nanofibers, respectively. Both nanofibers possess similar morphology with the average fiber diameter of about 300 nm. However, totally different crystalline structure is formed in these nanofibers, as seen from the WAXD profiles in Figure 1c. PLLA nanofiber shows diffraction peaks at 2θ = 15.1, 16.5 (assigned to (110)/(200)), and 18.1° that are assigned to α-form homocrystal of PLA.[12] On the other hand, stereocomplexed PLA nanofiber showed diffraction peaks at 2θ = 12.0 (assigned to (110)), 20.8, and 24.1° that are assigned only to stereocomplex crystal of PLA.[12]

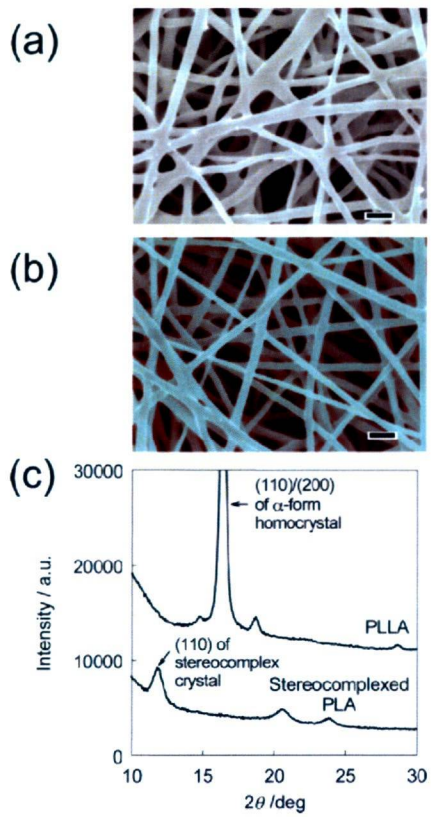

Figure 1. SEM images of (a) PLLA and (b) stereocomplexed PLA nanifibers and (c) wide-angle X-day diffraction patterns of PLLA and stereocomplexed PLA nanofibers. Scale bars = 1 μm. PLLA nanofiber shows diffraction peaks at 2θ = 15.1, 16.5 (assigned to (110)/(200)), and 18.1° that are assigned to α-form homocrystal of PLA. On the other hand, stereocomplexed PLA nanofiber showed diffraction peaks at 2θ = 12.0 (assigned to (110)), 20.8, and 24.1° that are aasigned only to stereocomplex crystal of PLA.

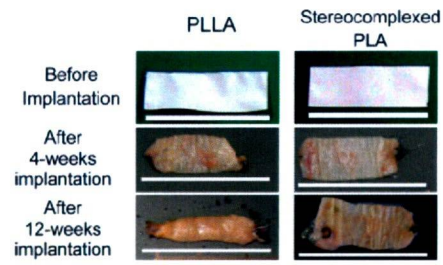

Figure 2. Bulk appearances of the nanofiber mats of PLLA and stereocomplexed PLA (a) before implantation, (b) after 4 weeks of implantation and (c) after 12 weeks of implantation. Scale bars = 3 cm.

This shows that the stereocomplexed PLA nanofiber consists of only the stereocomplex crystal and does not contain homocrystal of PLLA and PDLA at all.

The bulk appearances of the nanofiber mats were observed before and after removing the surrounding tissues. Figure 2 shows the photographs of nanofiber mats before and after 4 week and 12 week implantations, respectively. Significant reduction in the size of the PLLA nanofiber mat was recognized with the increasing period of implantation. In particular, the PLLA nanofiber mat after a 12 week implantation was densely covered with the surrounding tissues and only small fragments of the nanofibers mat were recovered. On the other hand, the stereocomplexed PLA nanofiber mat showed a less degree of the reduction in size than the PLLA nanofiber mat. This suggests that the in vivo degradation of the stereocomplexed PLA nanofiber mat occurs slower than the PLLA nanofiber mat.

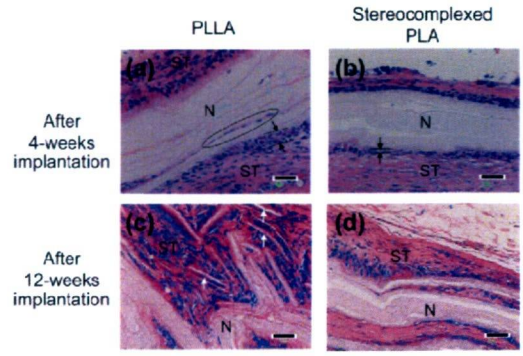

Figure 3. Histological images of PLLA and stereocomplexed PLA nanofibers before and after 4 weeks of implantation. (a) PLLA, before implantation; (b) stereocomplexed PLA, before implantation; (c) PLLA, after implantation; (d) stereocomplexed PLA, after implantation. Tissues were stained with hematoxylineosin. Nuclei of the inflammatory cells are stained blue. The width of inflammatory cells is indicated by the arrows and lines in (a) and (b). Ellipsoid region in (a) and white arrows in (c) indicate the infiltration of surrounding tissues and fragmented nanofibers, respectively. ST: surrounding tissues; N: nanofiber mats. Scale bars = 50 μm.

Histological Observation of Nanofiber Mats with the Surrounding Tissues. Histological observations of the nanofiber mats were performed to investigate the degree of inflammatory reactions and penetration of the surrounding tissues into the nanofiber mats. Figure 3 shows the phase contrast images of ultrathin sections of the explanted nanofiber mats stained by hematoxylin-eosin. The nuclei of inflammatory cells were stained blue by the hematoxylin dye and their presence is an indication of tissue response toward the implanted nanofiber mats. As indicated by the arrows and lines in Figure 3a, a thick layer of inflammatory cells was accumulated at the interface between the PLLA nanofiber mat and the surrounding tissues. In contrast, the layer of accumulated inflammatory cells was thinner for the stereocomplexed PLA nanofiber mat, as shown in Figure 3b. This indicates that the stereocomplexed PLA nanofiber mat causes smaller degree of inflammatory reactions than the PLLA nanofiber mat.

Furthermore, delamination (indicated by the ellipsoid in Figure 3a) occurred on the surface of the PLLA nanofiber mat, and hence, the infiltration of the surrounding tissues was observed. However, no infiltration of the surrounding tissues was observed for the stereocomplexed PLA nanofiber mat. After 12 weeks of implantation, while the PLLA nanofiber mat was significantly fragmented (white arrows indicate the fragmented nanofiber mat), the stereocomplexed PLA nanofibers retained the mat-like bulk morphology. These trends are well correlated with the bulk appearances of the nanofiber mats and support the observation that the in vivo degradation of the stereocomplexed PLA nanofiber mat proceeds slower than the PLLA nanofiber mat.

SEM Observation. SEM observation was performed for the nanofiber mats before and after 4 weeks and 12 weeks of implantation. Figure 4 shows the SEM images of nanofiber mats before implantation, after implantation and incubation at different periods of time. As for PLLA, cleavage of each strand of nanofiber occurred after 4 weeks. Furthermore, after 12 weeks, a decrease in the density of the nanofiber mat was observed. This is consistent with the histological image showing the fragmentation of the PLLA nanofiber mat. On the other hand, no cleavage of the stereocomplexed PLA nanofibers was observed even after 12 weeks of implantation.

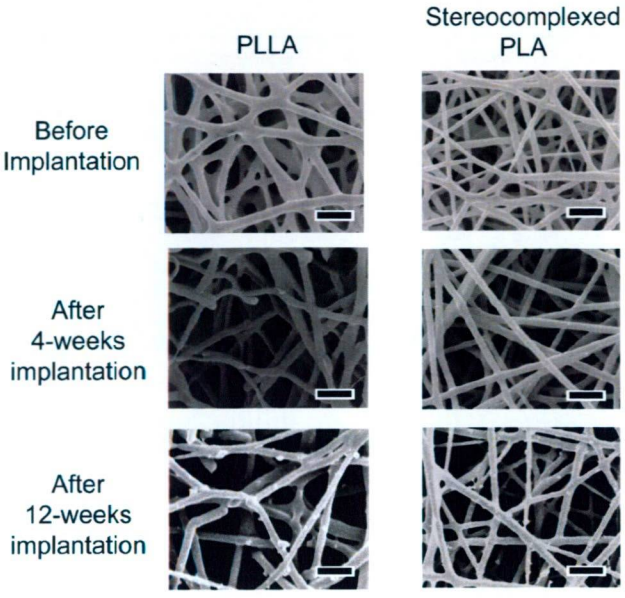

Figure 4. SEM images of PLLA (left) and stereocomplexed PLA (right) nanofibers. Upper row, before implantation; middle row, after 4 weeks of implantation; lower row, after 12 weeks of implantation. The surrounding tissues were removed by trypsin treatment. Scale bars = 1 μm.

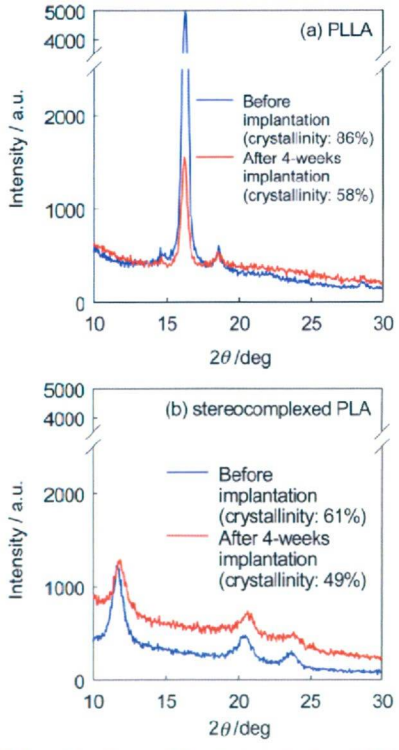

Figure 5. Wide-angle X-ray diffraction patterns of PLLA and stereocomplexed nanofibers before and after 4 weeks of implantation. PLLA nanofiber showed diffraction peaks at 2θ = 15.1°, 16.5°, and 18.1° that are assigned to homopolymer crystal of PLLA. On the other hand, stereocomplexed PLA nanofiber showed diffraction peaks at 2θ = 12.0, 20.8, and 24.1° that are assigned to stereocomplexed crystal. No diffraction peaks assigned to homopolymer crystal were observed in stereocomplexed PLA nanofiber.

Changes in Crystallinity. Figure 5 shows the WAXD patterns of the PLLA and stereocomplexed PLA nanofibers before and after 4 weeks of implantation. While the PLLA nanofiber showed diffractions that are assigned to the α-form crystal of PLA, the stereocomplexed PLA nanofiber showed diffractions assigned only to stereocomplexed crystal.[12] The crystallinity of both nanofibers was calculated as the ratio between the integrals of crystalline diffraction intensity and the total diffraction intensity. While the PLLA nanofiber showed considerable decrease in its crystallinity from 86 to 58%, the stereocomplexed PLA nanofiber showed a smaller decrease from 61 to 49%. These results show that the crystallinity of the stereocomplexed PLA is not so much lowered by implantation, while that of PLLA nanofiber significantly decreases. These results support the higher stability of stereocomplexed PLA nanofiber than PLLA nanofiber, as seen from visual inspection of the explanted nanofiber mat and the histological observation.

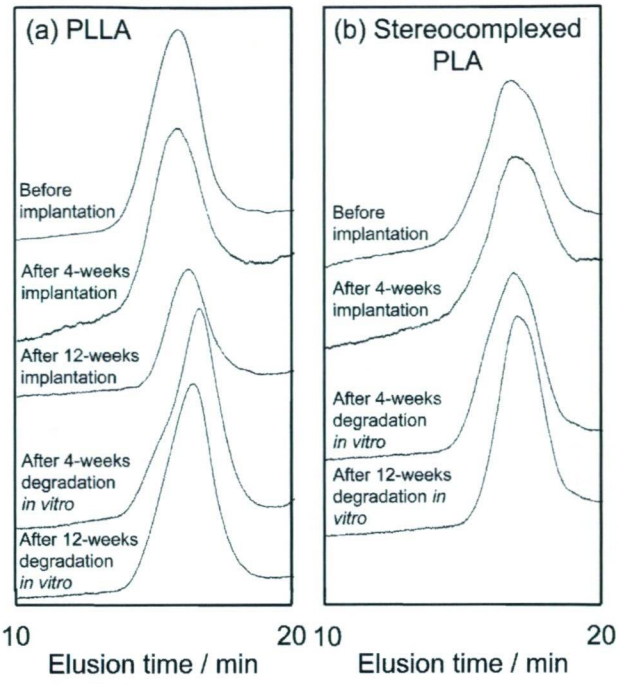

Figure 6. GPC elusion profiles of (a) PLLA and (b) stereocomplexed PLA nanofibers before and after implantation in vivo for 4 weeks and 12 weeks and before and after in vitro degradation for 4 weeks and 12 weeks.

GPC Analysis. The possibility of the cleavage of molecular chains during implantation, as suggested from SEM and WAXD data, was investigated by GPC analysis. The GPC elusion profiles are shown in Figure 6. Table 1 shows the number-averaged molecular weight, M_n, and the polydispersity index, M_w/M_n, of the PLLA and stereocomplexed PLA nanofibers before and after 4 weeks of implantation. Data for original PLLA are slso shown in Table 1. In the case of 12 weeks, GPC data of stereocomplexed PLA were not obtained because of its low solubility in chloroform. PLLA nanofiber showed a decrease in M_n during the implantation. In contrast, the M_n of stereocomplexed PLA nanofiber remained unchanged despite the decrease in M_w/M_n for 4 weeks of implantation. These results indicate that stereocomplexed PLA was not degradaded during implantation, while the PLLA chains in the nanofiber were considerably degraded. Additionally, in the case of the stereocomplexed PLA nanofiber, the extraction of low molecular weight fraction might occur during implantation.

In Vitro Degradation. To consider the results obtained from the in vivo experiment in terms of biocompatibility and bioabsorption, changes in the structure and properties of the nanofibers after in vitro incubation were investigated. As seen in Figure 7, both PLLA and stereocomplexed PLA nanofibers

Table 1. Number-Averaged Molecular Weight (M_n) and Polydispersity Index (M_w/M_n) of Original PLLA and PLA Nanofibers[a]

	PLLA		PDLA		stereocomplexed PLA	
	M_n	M_w/M_n	M_n	M_w/M_n	M_n	M_w/M_n
original	4.7×10^5	1.8	2.2×10^5	1.5		
nanofiber before implantation	3.8×10^5	2.3			8.7×10^4	3.3
after 4 weeks of implantation	3.0×10^5	2.4			8.6×10^4	2.3
after 12 weeks of implantation	1.7×10^5	2.3			[b]	[b]

[a] PLLA and stereocomplexed PLA before and after 4 weeks and 12 weeks of implantation. [b] Not obtained due to the poor solubility in chloroform.

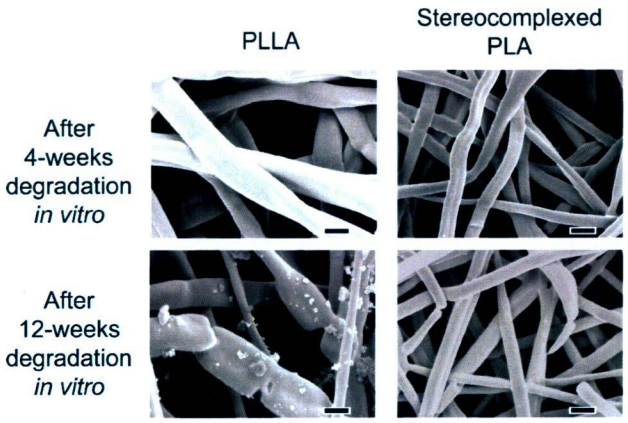

Figure 7. SEM images of PLLA (left) and stereocomplexed PLA (right) nanofibers after 4 weeks (upper) and 12 weeks (lower) in vitro degradation in PBS. Scale bars = 1 μm.

after in vitro incubation showed a considerable increase in the fiber diameter. This suggests that the significant swelling of the nanofibers occurred during the incubation. Interestingly, the stereocomplexed PLA nanofiber showed a smaller degree of swelling (from 300 to 600 nm) than the PLLA nanofiber (from 300 to 1200 nm). Because strong interaction works between molecular chains of PLLA and PDLA in the sterecomplexed PLA nanofiber, the swelling of the stereocomplexed PLA nanofiber might be suppressed.

GPC data of the nanofibers before and after in vitro degradation were also obtained, as shown in Figure 6b. The M_n and M_w/M_n estimated from the GPC curves are listed in Table 2. The M_n of stereocomplexed PLA was almost unchanged while that of PLLA showed a decrease from 3.8×10^5 to 1.8×10^5. These trends are consistent with the molecular weight data before and after the implantation in vivo as shown in Table 1.

The difference in the swelling behavior and molecular weight change in vitro between the stereocomplexed PLA and PLLA nanofibers may explain the results of the subcutaneous implantation in vivo in which the stereocomplexed PLA nanofiber showed smaller degree of absorption than the PLLA nanofiber.

Discussion

Degradation Mechanism of PLLA and Stereocomplexed PLA Nanofibers In Vivo. A schematic representation of the degradation mechanism of the PLLA and stereocomplexed PLA nanofibers is shown in Figure 8. For the PLLA nanofiber, it is believed that the molecular chains in the amorphous region between lamella crystals are preferentially hydrolyzed due to the intracrystalline swelling. This leads to the cleavage of a nanofiber and a decrease in the molecular weight. Then the chain-end degradation at the edge of the cleaved nanofiber may occur and lead to the decrease in the crystallinity. The cleavage of nanofiber may facilitate the delamination and the subsequent fragmentation of the nanofiber mats and, consequently, the infiltration of surrounding tissues in the PLLA nanofiber mat. Inflammatory reaction at the early stage may be due to the acidic low-molecular-weight degradation products and fragmented nanofibers.

A different situation was observed for the stereocomplexed PLA nanofibers. It is supposed that a single stereocomplexed PLA nanofiber is composed of PLLA and PDLA chains aligned

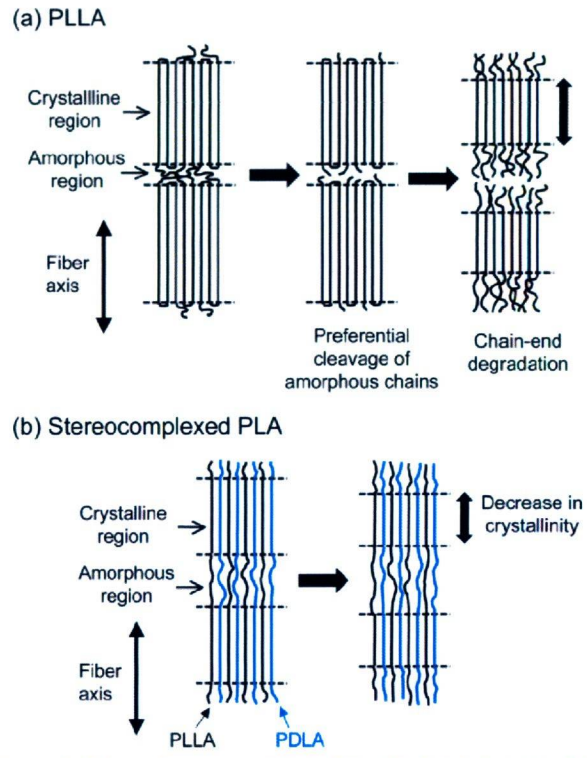

Figure 8. Schematic representation of the structural changes of (a) PLLA nanofiber and (b) stereocomplexed PLA nanofiber during implantation in vivo. For PLLA nanofiber, the amorphous chains between lamella crystals are preferentially hydrolyzed, leading to the cleavage of the nanofiber. Then, the chain-end degradation occurs at the edge of the cleaved nanofiber. Crystallinity of the PLLA nanofiber is thus considerably lowered. In contrast, degradation of stereocomplexed PLA is suppressed by the strong interaction between PLLA and PDLA chains, although the crystallinity slightly decreases.

Table 2. Number-Averaged Molecular Weight (M_n) and Polydispersity Index (M_w/M_n) of PLLA and Stereocomplexed PLA Nanofibers[a]

	PLLA		stereocomplexed PLA	
	M_n	M_w/M_n	M_n	M_w/M_n
before degradation	3.8×10^5	2.3	8.7×10^4	3.3
after 4 weeks of degradation	1.4×10^5	3.5	8.4×10^4	3.0
after 12 weeks of degradation	1.8×10^5	3.0	6.9×10^4	2.2

[a] Before and after 4 weeks and 12 weeks of degradation in vitro.

in a side-by-side manner. Accordingly, it is well-known that molecular interaction between PLLA and PDLA chains is strong, leading to higher melting temperature. Such molecular arrangement may suppress the hydrolysis of molecular chains in vivo. Thus, the stereocomplexed nanofiber morphology is retained. As a result, inflammatory reaction is limited at the vicinity of the interfacial region between nanofiber mats and the surrounding tissues.

General Discussion. Physiological response of tissues against implanted foreign materials is one of the most significant subjects to be considered in the development of medical biomaterials. In the case of polymeric biomaterials, the degree of the tissue responses, such as inflammatory reactions, partly depends on the chemical structure and, as a consequence, surface hydrophilic nature of the polymers.[23] Additionally, for biodegradable polymers, the degree of tissue responses is affected by the degradability in vivo.[24] For example, poly(glycolic acid) that undergoes degradation in vivo generally in 2−4 weeks is known to cause acute inflammatory reaction as the degradation proceeds.[25] It is known that the hydrolysis by body fluids is the major mechanism contributing in vivo degradation of polymeric biomaterials. We have already shown that the degradation behavior of poly(hydroxyalkanoate)s (PHAs) in vivo are largely affected by the monomer composition.[26] Nanofiber scaffolds made from these PHAs, ranging from poly[(*R*)-3-hydroxybutyrate] to poly[(*R*)-3-hydroxybutyrate-*co*-97 mol %-4-hydroxybutyrate] lead to contrasted tissue responses. The tissue responses were well correlated with the degradability of each polymer scaffolds. The present study using nanofibers of PLLA and stereocomplexed PLA suggested the correlation between the degree of inflammatory reaction in vivo and the change in the bulk size of each nanofiber mats. The changes in bulk size of the nanofibers were correlated to the changes in the microscopic morphology, crystallinity, and molecular weight. All these factors give evidence that the stereocomplexed PLA nanofibers are more stable and thus provoke lower degree of inflammation in vivo than the PLLA nanofibers.

In general, inflammatory reaction is favored in the case where healing occurs in a short period of time. For example, inflammatory reaction stimulates and accelerates the regeneration of some kinds of epithelial tissues. On the other hand, in the case where healing requires a longer time, chronic inflammatory response is not favored. For example, suppression of the inflammatory responses against artificial vessel has significance for treatment of the circulatory organs that requires a period of more than half a year. From this viewpoint, our results show that the stereocomplexed PLA nanofibers are suitable for the purposes where the chronic inflammatory reaction should be avoided, for example, guided nerve regeneration or blood vessel augmentation. On the other hand, conventional PLLA nanofibers may be suitable for the rapidly bioresorbable materials, for example, wound healing patches. Such versatility of the biodegradability would expand the potential of PLAs as biomaterials.

Conclusion

Fiber morphology, crystallinity, and molecular weight of PLLA and stereocomplexed PLA nanofibers before and after implantation in vivo were investigated using SEM, WAXD, and GPC. The stereocomplexed PLA nanofiber retained its fiber morphology, crystallinity, and molecular weight after a 12 week implantation. On the other hand, the PLLA nanofiber showed breakdown of the fiber morphology and significant decrease in crystallinity and molecular weight. The degree of inflammatory reaction against the nanofibers in vivo was correlated to the degradation behavior. The larger stability against hydrolysis of stereocomplexed PLA nanofiber, attributed to the strong interaction between PLLA and PDLA chains in the nanofiber, was confirmed by in vitro degradation.

Acknowledgment. This work has been supported by a grant provided for Ecomolecular Research II in RIKEN Institute (The Institute of Physical and Chemical Research), Japan, and by a Grant-in-Aid from the Ministry of Education, Culture, Sports, Science and Technology, Japan (No. 19350075, to T.I.). We thank Ms. Noreen Fundador for the English correction of our manuscript.

References and Notes

(1) Langer, R.; Vacanti, J. P. *Science* **1993**, *260*, 920–926.
(2) Reneker, D. H.; Chun, I. *Nanotechnology* **1996**, *7*, 216–223.
(3) Morota, K.; Matsumoto, K.; Mizukoshi, T.; Konosu, Y.; Minagawa, M.; Tanioka, A.; Yamagata, Y.; Inoue, K. *J. Colloid Interface Sci.* **2004**, *279*, 484–492.
(4) Murugan, R.; Ramakrishna, S. *Tissue Eng.* **2006**, *12*, 435–447.
(5) Buchko, C. J.; Chen, L. C.; Shen, Y.; Martin, D. C. *Polymer* **1999**, *40*, 7397–7407.
(6) Zong, X.; Kim, K.; Fang, D.; Ran, S.; Hsiao, B. S.; Chu, B. *Polymer* **2002**, *43*, 4403–4412.
(7) Zong, X.; Ran, S.; Kim, K.-S.; Fang, D.; Hsiao, B.; Chu, B. *Biomacromolecules* **2003**, *4*, 416–423.
(8) Ikada, Y.; Tsuji, H. *Macromol. Rapid Commun.* **2000**, *21*, 117–132.
(9) Iwata, T.; Doi, Y. *Sen'i Gakkaishi* **2001**, *57*, 172–177.
(10) Ikada, Y.; Jamshidi, K.; Tsuji, H.; Hyon, S. H. *Macromolecules* **1987**, *20*, 904–906.
(11) Tsuji, H. *Macromol. Biosci.* **2005**, *5*, 569–597.
(12) Okihara, T.; Tsuji, M.; Kawaguchi, A.; Katayama, K.; Tsuji, H.; Hyon, S. H.; Ikada, Y. *J. Macromol. Sci., Part B: Phys.* **1991**, *30*, 119–140.
(13) Tsuji, H. *Polymer* **2000**, *41*, 3621–3630.
(14) Tsuji, H.; Suzuki, M. *Sen'I Gakkaishi* **2001**, *57*, 198–202.
(15) Tsuji, H.; Miyaushi, S. *Biomacromolecules* **2001**, *2*, 597–604.
(16) Takasaki, M.; Ito, H.; Kikutani, T. *J. Macromol. Sci., Part B: Phys.* **2003**, *42*, 57–73.
(17) Furuhashi, Y.; Kimura, Y.; Yamane, H. *J. Polym. Sci., Part B: Polym. Phys.* **2007**, *45*, 218–228.
(18) Tsuji, H.; Nakano, M.; Hashimoto, M.; Takashima, K.; Katsura, S.; Mizuno, A. *Biomacromolecules* **2006**, *7*, 3316–3320.
(19) Ishii, D.; Lee, W.-K.; Kasuya, K.-I.; Iwata, T. *J. Biotechnol.* **2007**, *132*, 318–324.
(20) Kim, K.; Yu, M.; Zong, X.; Chiu, J.; Fang, D.; Seo, Y.-S.; Hsiao, B. S.; Chu, B.; Hadjiargyrou, M. *Biomaterials* **2003**, *24*, 4977–4985.
(21) Zeng, J.; Chen, X.; Liang, Q.; Xu, X.; Jing, X. *Macromol. Biosci.* **2004**, *4*, 1118–1125.
(22) You, Y.; Min, B.-M.; Lee, S. J.; Lee, T. S.; Park, W. H. *J. Appl. Polym. Sci.* **2005**, *95*, 193–200.
(23) Wang, Y.-X.; Robertson, J. L.; Spillman, W. B.; Claus, R. O. *Pharm. Res.* **2004**, *21*, 1362–1373.
(24) Hasirci, V.; Lewandrowski, K.; Gresser, J. D.; Wise, D. L.; Trantolo, D. J. *J. Biotechnol.* **2001**, *86*, 135–150.
(25) Ceonzo, K.; Gaynor, A.; Shaffer, L.; Kojima, K.; Vacanti, C. A.; Stahl, G. A. *Tissue Eng.* **2006**, *12*, 301–308.
(26) Tan, H. Y.; Ishii, D.; Mahara, A.; Murakami, S.; Yamaoka, T.; Sudesh, K.; Samian, R.; Fujita, M.; Maeda, M.; Iwata, T. *Biomaterials* **2008**, *29*, 1307–1317.

BM8009363

Modification of PLA Scaffolds Using Bioactive Peptide-Oligo (Lactic Acid) Conjugates

Sachiro Kakinoki[1,2], Sho Uchida[1,3], Tomo Ehashi[1,2], Akira Murakami[3], and Tetsuji Yamaoka[1,2]

[1]Department of Biomedical Engineering, National Cardiovascular Center Research Institute, 5-7-1 Fujishirodai, Suita, Osaka 565-8565, Japan, [2] JST, CREST, 5 Sanbancho, Chiyoda-ku, Tokyo 102-0075, Japan, [3] Department of Polymer Science and Engineering, Kyoto Institute of Technology, Kyoto 606-8585, Japan.
e-mail: yamtet@ri.ncvc.go.jp

A novel method for surface modification of PLA scaffold based on amphiphilic conjugates composed of oligo lactic acid (OLA) and bioactive peptide was designed and developed. PLA thin-films modified with the amphiphilic OLA-AG73 conjugates were prepared by spin-coating. Cell adhesion and neurite outgrowth of PC12 cells on the modified thin-films were greatly improved.

Keywords: AG73, nerve regeneration, PLA, scaffolds, surface modification

Introduction

Tissue engineering has been proposed as an approach to create tissues and organs by use of various scaffolds as a temporary extra-cellular matrix. Poly (lactic acid) (PLA) is a preferred biodegradable material since it is non-enzymatically hydrolyzed to low-toxic lactic acid *in vivo* and has high mechanical properties and excellent shaping and molding properties.

On the other hand, PLA has no specific bioactivities and then is preferred to be modified with bioactive molecules. A variety of bioactive peptides has been reported to be useful for tissue regeneration so far. For example, RGD sequence isolated from fibronectin is well known to support cell adhesion. Various modification techniques for PLA which has no functional groups have been proposed [1] but they are quite hard to apply to the nano-stractured PLA scaffold since they are very fragile. In this report, we developed amphiphilic conjugates composed of bioactive peptides and oligo (lactic acid) (OLA) to functionalize nano-stractured PLA scaffolds and evaluate their bioactivities.

Results and Discussion

Bioactive sequence, RKRLQVQLSIRT (AG73) [2], which has been reported to accelerate the neurite outgrowth *in vitro* was selected. OLA whose hydroxyl group end is capped with acetyl group was synthesized by condensation reaction. The OLA-AG73 conjugates were synthesized by Fmoc solid phase procedure (Scheme 1).

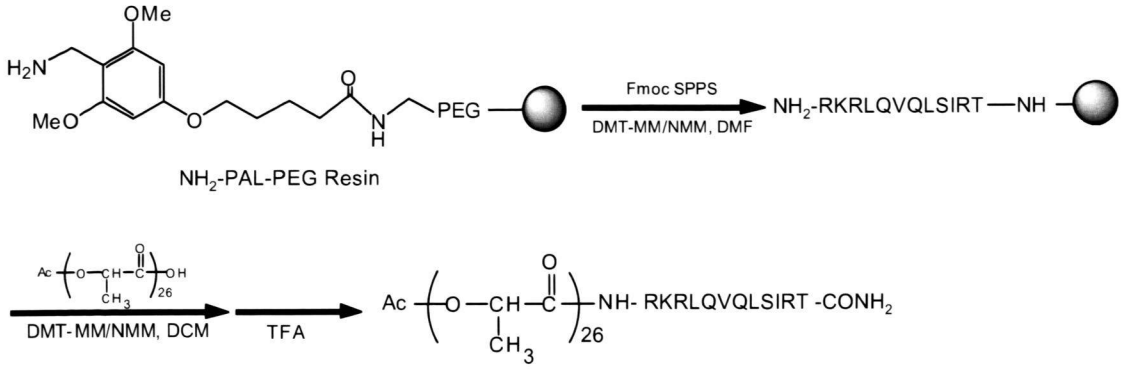

Scheme 1. Synthesis of Ac-OLA26-AG73.

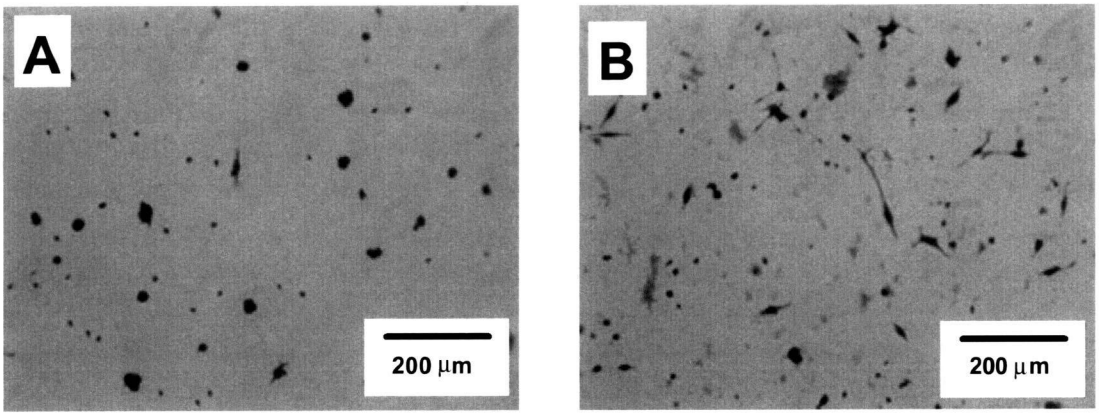

Figure 1. Neurite outgrowth of PC12 cells on PLA (A) and PLA/OLA-AG73 (B) thin-films.

Three weight % of OLA-AG73 conjugates were added to 10 weight % of PLA solution in hexafluoro isopropanol, and the mixed solutions were spin coated onto cover glass (φ 14 mm) or electro spun to aluminum foil, resulting in surface modified thin-films and nano-fiber sheets respectively. As is shown in Figure 1, the cell adhesion and neurite outgrowth of PC12 cells on PLA/OLA-AG73 thin-film were improved and reached to longitudinal and transversal respectively. These behaviors must be resulted from AG73 peptides immobilized on thin-film surface but other factors may also affect it. The physicochemical characteristics should be changed even when only 3 % of OLA-AG73 was added. In addition, the surface density of OLA-AG73 on thin-film and its releasing profiles should be analyzed in detail.

In general nano-stractured PLA scaffolds are much more difficult to be modified than the bulk materials because they are very weak and fragile against to mechanical stress, chemical reaction, and thermal treatment. The newly developed OLA-Peptide conjugates were found to be very powerful tool for modifying such ultra thin-films or nano-fibers just by adding only 3 % to the dope before processing.

References

1. Fujiwara T., Mukose T., Yamaoka, T., Yamane H., Sakurai S., Kimura Y. (2001) *Macromol. Biosci.*, **1**, 204-208.
2. Weeks B. S., Nomizu M., Ramachandran R.S., Yamada Y., Kleinman H. K. (1998) *Exp. Cell Res.*, **243**, 375-382.

Circulation
JOURNAL OF THE AMERICAN HEART ASSOCIATION

American Heart Association®
Learn and Live℠

Oppression of Left Main Trunk Due to Pseudoaneurysm With Graft Detachment in Patients With Behcet Disease Previously Treated by Bentall Procedure

Yu Kataoka, Takeshi Tsutsumi, Kouhei Ishibashi, Masahiro Higashi, Isao Morii, Atsushi Kawamura, Hatsue Ishibashi-Ueda, Kenji Minatoya, Hitoshi Ogino and Yoritaka Otsuka

Circulation 2009;119;2858-2859
DOI: 10.1161/CIRCULATIONAHA.108.803387
Circulation is published by the American Heart Association. 7272 Greenville Avenue, Dallas, TX 72514
 Print ISSN: 0009-7322. Online ISSN: 1524-4539

Oppression of Left Main Trunk Due to Pseudoaneurysm With Graft Detachment in Patients With Behcet Disease Previously Treated by Bentall Procedure

Yu Kataoka, MD; Takeshi Tsutsumi, MD; Kouhei Ishibashi, MD; Masahiro Higashi, MD; Isao Morii, MD; Atsushi Kawamura, MD; Hatsue Ishibashi-Ueda, MD; Kenji Minatoya, MD; Hitoshi Ogino, MD; Yoritaka Otsuka, MD

A 35-year-old Japanese man was admitted to our hospital because of congestive heart failure in January 2006. Echocardiography showed severe aortic regurgitation and partial ruptured aneurysm of the Valsalva sinus. Because he had already presented oral aphthae, uvetis, skin lesions with bouton, and genital ulceration, this case was diagnosed as a complete form of Behcet disease and the Bentall operation was performed. He was discharged without any complications. However, he experienced chest pain with ST-segment depression 3 months after the Bentall operation although no significant stenosis could be seen by preoperative coronary angiography in January 2006. This patient had III/VI systolic murmur of intensity of Levine on the third left sternal border. Transthoracic and transesophageal echocardiography revealed the echo-free space around the aortic graft and an abnormal jet from the left ventricular outflow to that echo-free space (online-only Data Supplement Movies I and II). Multislice computed tomography showed the development of

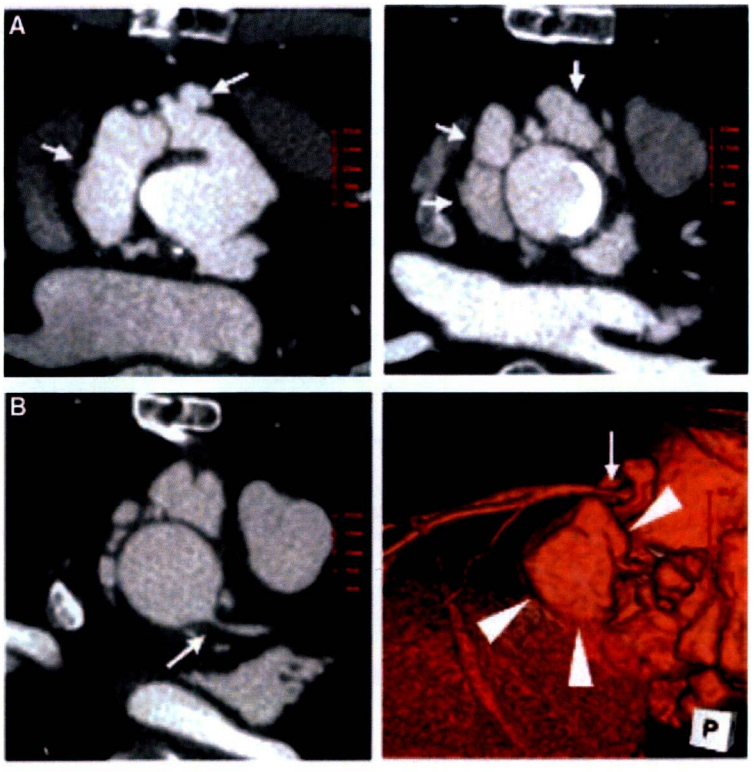

Figure 1. A, Multislice computed tomography reveals the development of multiple pseudoaneurysms around the aortic graft (arrows). B, One of those pseudoaneurysms oppresses the left main trunk (triangle) and causes severe stenosis (arrows).

From the Division of Cardiology (Y.K., T.T., K.I., Y.O.), Cardiovascular Surgery (K.M., H.O.), Radiology (M.H.), and Pathology (H.I.), National Cardiovascular Center, Osaka, Japan; Division of Cardiology, Hokusetsu General Hospital, Takatsuki, Japan (I.M.); and Division of Cardiology, Central Hospital, Hiroshima, Japan (A.K.).

The online-only Data Supplement is available with this article at http://circ.ahajournals.org/cgi/content/full/119/21/2528/DC1.

Address for correspondence: (current address), Yu Kataoka, MD, Division of Cardiology, Department of Medicine, National Cardiovascular Center, 5-7-1 Fujishiro-dai, Suita, Osaka 565-8565, Japan. Tel:81-6-6833-5012, Fax:81-6-6872-7486, Email: kataoka@hsp.ncvc.go.jp

(*Circulation.* 2009;119:2858-2859.)

***Circulation* is available at http://circ.ahajournals.org** **DOI: 10.1161/CIRCULATIONAHA.108.803387**

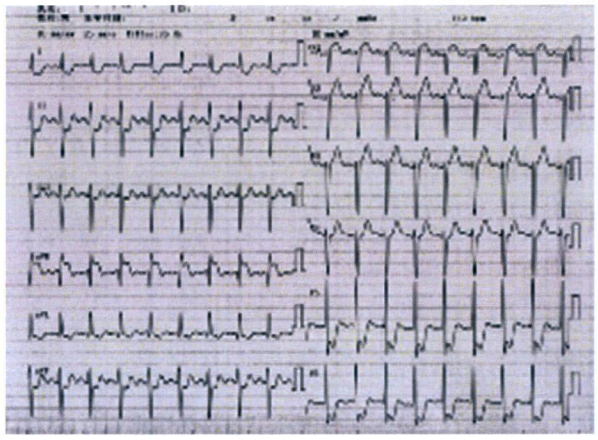

Figure 2. ECG demonstrates the presence of severe ischemic change on day 5 after admission.

multiple pseudoaneurysms around the aortic graft, which oppressed the left main trunk and caused severe stenosis of the left main trunk (Figure 1A and 1B). Because he had progressive angina with severe ST-segment changes (Figure 2), the Bentall operation was reperformed on an urgent basis, in addition to coronary artery bypass grafting. The aortic graft was detached at the right coronary cusp and multiple pseudoaneurysms were seen at the right and left coronary cusps. In addition, a pseudoaneurysm at the left coronary cusp oppressed the left main trunk, and severe stenosis in the left main trunk was observed. After the previously implanted composite graft was resected, new composite graft was implanted into the annulus. The left coronary ostia was reimplanted using the button technique, and coronary artery bypass grafting was performed for the right coronary artery. Histological examination of the explanted synthetic graft of the aortic root revealed poor organization with severe inflammatory cell infiltration such as neutrophils and macrophages (Figure 3). Numerous Gram-positive cocci were also recognized in the graft (Figure 3).

Graft detachment or pseudoaneurysm after the Bentall operation in Behcet disease occurs in 20% to 40% of cases.[1,2] However, there are no case reports like the present case. In this case, the inflammation level was not satisfactorily controlled and the C-reactive protein level on admission was high (9.6 mg/dL). Therefore, inflammation leading to fragility of the aortic wall seems to cause these rare complications. After reoperation and strict control of inflammation using methylprednisolone, the patient had no recurrence of psuedoaneurysm formation during a 2-year follow-up period.

Acknowledgments

We would like to thank Mrs Hiromi Maeda for her excellent secretarial assistance, and the nurses and residents in the coronary care unit of the National Cardiovascular Center for their cooperation.

Disclosures

None.

References

1. Ando M, Kosakai Y, Okita Y, Nakano K, Kitamura S. Surgical treatment of Behcet's disease involving aortic regurgitation. *Ann Thorac Surg.* 1999;68:2136–2140.
2. Alpagut U, Ugurlucan M, Dayioglu E. Major arterial involvement and review of Behcet's disease. *Ann Vasc Surg.* 2007;21:232–239.

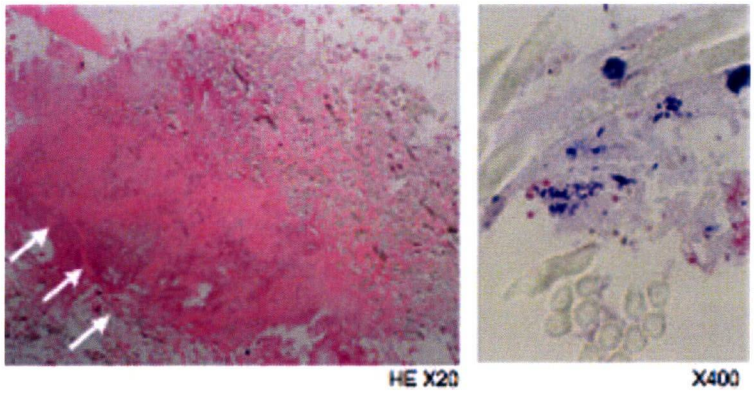

Figure 3. Histological examination of the explanted synthetic graft of the aortic root reveals poor organization with severe inflammatory cell infiltration such as neutrophils and macrophages (left, arrows). Numerous Gram-positive cocci were also recognized in the graft (right).

Original Article

Is Prompt Surgical Treatment of an Abdominal Aortic Aneurysm Justified for Someone in Their Eighties?

Masato Tochii, MD,[1,2] Hitoshi Ogino, MD,[1] Hitoshi Matsuda, MD,[1] Kenji Minatoya, MD,[1] Hiroaki Sasaki, MD,[1] and Soichiro Kitamura, MD[1]

Objectives: The aim of this study is to review the early and long-term results and quality of life after abdominal aortic aneurysm (AAA) surgery in octogenarians to justify our prompt surgical intervention.

Patients and Methods: We reviewed the consecutive 444 patients who underwent graft replacement of AAA in our center from October 1997 to September 2002. The median age of the patients was 72.3. An elective operation was carried out in 401 cases (90.3%) and an emergency operation in 43 cases (9.7%). We evaluated the early and long-term results of AAA surgical treatment, including the quality of life after hospital discharge.

Results: There were 12 hospital deaths (2.7%) in the early outcomes, 11 of which (25.6%) were during emergency operations, and only one patient (0.2%) died among the elective cases ($p < .0001$). In the early results, the emergency operation ($p = 0.0001$) was the only risk factor in the early deaths investigated by the multivariate logistic regression; patients aged 80 years and over did not constitute a risk factor. There were 36 late deaths, but none related to AAA surgical treatment. The strongest predictors for late mortality included patients aged 80 years and over ($p = 0.027$), male gender ($p = 0.048$), chronic renal failure with preoperative serum creatinine level equal to or greater than 1.5 mg/dl ($p = 0.043$), a history of atherosclerotic obliterans ($p = 0.009$), and an emergency operation ($p < .001$) investigated by the Cox hazard multivariate logistic regression. Among the survivors, 86.1% of the patients aged 80 years and over were able to maintain their previous lifestyles with the independent activities of everyday life.

Conclusions: AAA surgical treatment in octogenarians had comparable results with younger patients, in either elective or emergency settings. The extension of indications for AAA elective surgery in octogenarians might lead to a lower rate of emergency settings and subsequently to better early and late surgical outcomes. (Ann Thorac Cardiovasc Surg 2009; 15: 23–30)

Key words: abdominal aortic aneurysm, octogenarian, surgical treatment

Introduction

Surgical indication for abdominal aortic aneurysm (AAA) in elderly patients depends on the risk of the operation compared with the risk of rupture of the unoperated aneurysm in the natural course of events. However, the surgical risk tends to rise with age because of the increase in the prevalence of various diseases associated with declines in the homeostatic reserve. Our principle is not to deny AAA surgical

From [1]Department of Cardiovascular Surgery, National Cardiovascular Center, Suita, and [2]Department of Cardiovascular Surgery, Fujita Health University, Toyoake, Japan

Received January 29, 2008; accepted for publication February 12, 2008

Address reprint requests to Hitoshi Ogino, MD: Department of Cardiovascular Surgery, National Cardiovascular Center, 5–7–1 Fujishirodai, Suita, Osaka 565–8565, Japan.

treatment even in patients aged 80 years and over if the surgical risk would not exceed the risk of rupture, and if the surgery would not impair the quality of life. The aim of this study is to review early and long-term results, including the quality of life after AAA surgical treatment in octogenarians, to justify our prompt surgical intervention.

Patients and Methods

We reviewed the consecutive 444 patients who underwent graft replacement of AAAs in our center during a 5-year period, from October 1997 to September 2002. All patients had infrarenal AAAs and underwent in-situ graft replacements of the aneurysm. Patients having suprarenal AAAs, redo cases, and patients undergoing concomitant coronary artery bypass grafting were excluded from this study. The patients' profiles are shown in Table 1. This study includes all 444 cases. Male patients comprised 83.3% of the cases, and the male-to-female ratio was 4:1. An elective operation was carried out in 401 cases (90.3%), and an emergency operation in 43 (9.7%). In the emergency settings, there were 30 cases of a ruptured AAA and 13 of an impending ruptured AAA. The median age of patients was 72.3, ranging from 49 to 89. Octogenarian patients numbered 69 (15.5%), and 375 of all the patients (84.5%) were less than 80 years old. The ratio of emergency operations was significantly higher ($p = 0.003$) in the octogenarians (20.3%; 14/69), but only 7.7% (29/375) in patients younger than 80. Two cases, aged 85 and 87, had a previous history of stent graft implantation for the AAA. They had undergone surgical treatment 2 years after the stent grafting. One patient underwent an elective operation for the severe coagulopathy resulting from a type I endoleak of the previous stent, and the other underwent an emergency operation for AAA rupture. The maximum diameter of the aneurysm was 54.9 ± 10.3 (35–110) mm. The past history is also shown in Table 1. Ischemic heart disease was detected in 182 cases (41.0%), 68 of which had undergone percutaneous coronary intervention, and 45 had a previous history of coronary artery bypass grafting. Thirty patients were suffering from chronic renal failure, and 8 had been maintained with hemodialysis. We evaluated the early and long-term results of AAA surgical treatment. Surgical treatment was indicated for aneurysms larger than 45 mm, even for smaller ones with expansion rates exceeding 10 mm per year, and for all cases of ruptured or impending rupture of the aneurysm. The emergency settings included ruptured and impending ruptured AAAs. An impending AAA rupture was defined as a nonruptured, large symptomatic AAA that had undergone graft replacement within 24 hours after the diagnosis.

Table 1. Patients' profiles

	Number of patients	%
Total	444	
Male gender	370	83.3
Age	72.3 ± 7.6 (49–89) years	
Maximum diameter	54.9 ± 10.3 (35–110) mm	
Elective	401	90.3
Emergency: rupture	30	6.8
Emergency: impending rupture	13	2.9
Hypertension	351	79.1
Hyperlipidemia	243	54.7
Diabetes mellitus	55	12.4
Cerebrovascular disease	50	11.3
Ischemic heart disease	182	41.0
COPD	36	8.1
Chronic renal failure (Cr ≥ 1.5 mg/dl)	30	6.8
maintained by HD	8	1.8
TAA/TAAA	27	6.1
Aortic dissection	29	6.5
Atherosclerotic obliterans	27	6.1

COPD, chronic obstructive pulmonary disease; Cr, creatinine; HD, hemodialysis; TAA/TAAA, thoracic and/or thoracoabdominal aortic aneurysm.

Our strategy involves performing dipyridamole myocardial scintigraphy for preoperative evaluation of coronary artery disease in all cases in elective settings. This is followed by coronary angiography only for patients having positive findings of myocardial ischemia detected by the scintigram, and having past histories of coronary artery disease or of surgical or catheter intervention. In a case of significant coronary artery stenoses, a catheter intervention or coronary artery bypass grafting was performed before AAA surgery. Coronary artery bypass grafting was carried out simultaneously with graft replacement of the AAA for patients having a large AAA (greater than 70 mm) and/or severe coronary artery disease. These patients having concomitant surgery were excluded from this study.

Clinical data collection, definition, and follow-up

The data were collected from the medical records. The preoperative complications and past histories were

defined as the following criteria: (1) ischemic heart disease included myocardial infarction with a history of enzymatic elevation and echocardiographic signs of necrosis and angina pectoris diagnosed by coronary angiography and scintigraphy; (2) chronic obstructive pulmonary disease with less than 70% of forced expiratory volume in one second; (3) chronic renal failure with serum creatinine (Cr) level equal to or more than 1.5 mg/dl; (4) thoracic and/or thoracoabdominal aortic aneurysm (TAA/TAAA); unoperated aneurysm over 40 mm in diameter; (5) past history of aortic dissection; (6) atherosclerotic obliterans for patients having intermittent claudication with significant arterial stenosis. Mortality in the early results included hospital deaths from all causes. The surviving patients were followed up in our outpatient clinic or other local clinic after hospital discharge. The most recent information was obtained by mailing and calling the patients or their families. For looking at the long-term outcome, we mailed a questionnaire to all patients who had survived the operation and returned home. Recent information about patients whose addresses were uncertain was obtained from their most recent clinical records. We asked the patients or their families about the clinical histories and daily activities after discharge and, if the patient had died, the cause of death and time. The end point of the late outcome was defined as death from any cause.

Statistical analysis

The results were expressed as mean ± standard deviation. A statistical analysis comparing the two groups was performed with an unpaired two-tailed Student's *t*-test for the means or χ^2 test for categorical variables, for which the relative risk with 95% confidence interval was calculated. The two-sided p values were calculated with Pearson's χ^2 test or, if expected frequencies fell below 5, with Fisher's χ^2 test. The actual survival curve was obtained by the Kaplan-Meier life table method, and statistical analysis was calculated with the log-rank test. The Cox hazard analysis model was used to evaluate the independent risk factors of the early and late results. Stepwise logistic regression was used to select the independent variables that could predict stronger factors for the early and late outcomes and included all the univariate variables with a p value less than or equal to 0.2. Independent variables were expressed as an odds ratio (OR), and the related p value was also reported. Significant factors from the univariate analysis were then entered into the multivariate analysis. In the Cox hazard model, the independent variables were expressed as an odds ratio, and the related p value and 95% confidence interval (95% CI) were also reported. The p values less than or equal to 0.05 were considered a statistically significant difference.

Table 2. Early outcome

Hospital death	12/444	2.7%
Elective	1/401	0.2%
Rupture	10/30	33.3%
Impending rupture	1/13	7.7%
Major complication	52/444	11.7%
Blood transfusion	246/444	55.4%
Operation time	266.5 ± 91.7 mins	
Hospital stay (survivors only)	20.5 ± 14.0 days	

Results

Early outcome

There were 12 hospital deaths (2.7%) in the early results (Table 2). Among the elective cases, only one patient died (0.2%). This patient had previously undergone bifurcated stent implantation because at 85 years of age he was considered to be a very high-risk patient for surgery. Elective graft replacement was required because of severe coagulopathy resulting from a type I endoleak at the proximal portion of the previous stent, but he expired from multiple organ failure. Among 30 cases of ruptured aneurysm, 10 patients died (33.3%) during their hospital stay. The causes of death were bowel necrosis in 4 patients and renal failure in 2. The other 4 patients, who had suffered from cardiac arrest before the operation and emergency laparotomy under cardiopulmonary resuscitation, died because of multiple organ failure, though the graft replacement had been successful. The remaining patient had died of impending aneurysm rupture, pan peritonitis from the previously inserted peritoneal dialysis catheter. Major complications occurred in 52 patients (11.7%) (Table 3). The incidence of fatal complications after the surgical treatment—heart failure, respiratory insufficiency requiring a tracheotomy, acute renal failure requiring hemodialysis, and bowel necrosis—was significantly higher in the emergency cases (p <.0001, respectively). Bowel necrosis was observed in 4 patients with ruptured AAAs, and a laparotomy was carried out in the 4. They all died, though a colectomy had been successfully performed on 2. Colon resection could not be carried out for the